Journal of Hazardous Materials 192 (2011) 1466–1475

Contents lists available at ScienceDirect

Journal of Hazardous Materials

journal homepage: www.elsevier.com/locate/jhazmat

Mobilization and deposition of iron nano and sub-micrometer particles in porous media: A glass micromodel study

Qiliang Wang[a], Jung-Hyup Lee[a], Seung-Woo Jeong[b,**], Am Jang[a], Sanghyup Lee[c], Heechul Choi[a,*]

[a] School of Environmental Science and Engineering, Gwangju Institute of Science and Technology (GIST), 261 Cheomdan-gwagiro, Buk-gu, 500-712 Gwangju, Republic of Korea
[b] Department of Environmental Engineering, Kunsan National University, Kunsan, Republic of Korea
[c] Center for Environmental Technology Research, Korea Institute of Science and Technology, 130-650 Seoul, Republic of Korea

ARTICLE INFO

Article history:
Received 24 January 2011
Received in revised form 22 June 2011
Accepted 24 June 2011
Available online 18 July 2011

Keywords:
Iron nanoparticles
Glass micromodel
Mobilization-deposition
Humic substances
DLVO theory

ABSTRACT

Mobilization and deposition of iron nano and sub-micrometer particles (INSMP) in a porous medium were investigated using a water-saturated glass micromodel. The deposition and detachment of INSMP in the micromodel were visualized by taking serial images and experimentally verified by analysis of breakthrough curves. This first visualization study of INSMP fate showed that there were dense aggregations at the pores as the concentration of INSMP increased. The presence of dissolved humic substances (>1 ppm) significantly reduced deposition of suspended particles and enhanced detachment of the deposited particles. The mobility of INSMP in the presence of Pahokee peat fulvic acid standard II (PPFA) was higher than for Pahokee peat humic acid standard I (PPHA) due to the presence of more aromatic groups and the molecular weight in PPFA. Interfacial energy estimation based on the DLVO theory revealed that the adsorption of humic substances onto the INSMP increased the energy barrier and reduced the depth of secondary minimum between particles. The "affinity transition" in the initial deposition of INSMP within the micromodel was observed in the presence of Pahokee peat humic substances.

1. Introduction

The application of iron nanoparticles for environmental remediation has recently been receiving a great deal of attention [1–7], e.g., iron nanoparticles are widely used for dechlorination of chlorinated compounds and immobilization of heavy metals in groundwater [8–10]; additionally, Noubactep and his colleagues have challenged the view that iron nanoparticles are reducing agents shown that contaminants are basically removed by adsorption and co-precipitation [11,12]. The large surface area and reactivity of iron nanoparticles can be applied to a promising and flexible technology for in situ remediation of groundwater contaminants [8]. Iron nanoparticles having small particle size compared to soil pores show much potential for enhanced transport to contamination source zones [13,14]. However, recent studies have reported that bare iron nanoparticles have a strong tendency to agglomerate due to their high surface energy and intrinsic magnetic interactions, forming aggregates that plug and inhibit their mobility through porous media [15,16].

Conventionally, the stability and deposition of colloid particles are described using Derjaguin and Landau, Verwey and Overbeek (DLVO) theory and deep bed filtration model [15,17–20]. In DLVO theory, colloid particle stability is promoted by the existence of an energy barrier in the inter-particle interaction potential. Moreover, DLVO theory assumes mono-dispersed particles and irreversible attachment in a primary minimum, whereas surface modified colloid particles are likely to be deposited within a secondary minimum, which is subject to detachment under an external force (e.g., shear force) [21]. Lab-synthesized iron nanoparticles have an Fe^0 core and an iron oxides shell. These iron particles are polydispersed and have magnetic properties between the particles to affect the dispersion stability [16,22,23]. Therefore, it has been expected that classical DLVO theory alone is not appropriate for prediction of interactions of iron nanoparticles. In the deep bed filtration model, the attachment efficiency is controlled by collector interactions and is independent of particle concentration. Particle deposition to the previously attached particles (e.g., blocking and ripening) and agglomeration due to magnetic attractive forces are neglected in the theory [18–20,24,25].

Natural organic matter (NOM) is a complex mixture of many molecules. A large portion of NOM is present as humic acid (HA) and fulvic acid (FA) [26]. Due to its complex nature, NOM should be treated as different components in adsorption and transport studies. Interactions between NOM and iron-nanoparticles would result in a reduced sticking coefficient (scavenging by attachment) to

* Corresponding author. Tel.: +82 62 715 2441; fax: +82 62 715 2434.
** Co-corresponding author. Tel.: +82 63 469 4767; fax: +82 63 469 4964.
E-mail addresses: swjeong@kunsan.ac.kr (S.-W. Jeong), hcchoi@gist.ac.kr, hcchoi@kjist.ac.kr (H. Choi).

0304-3894/$ – see front matter © 2011 Elsevier B.V. All rights reserved.
doi:10.1016/j.jhazmat.2011.06.066

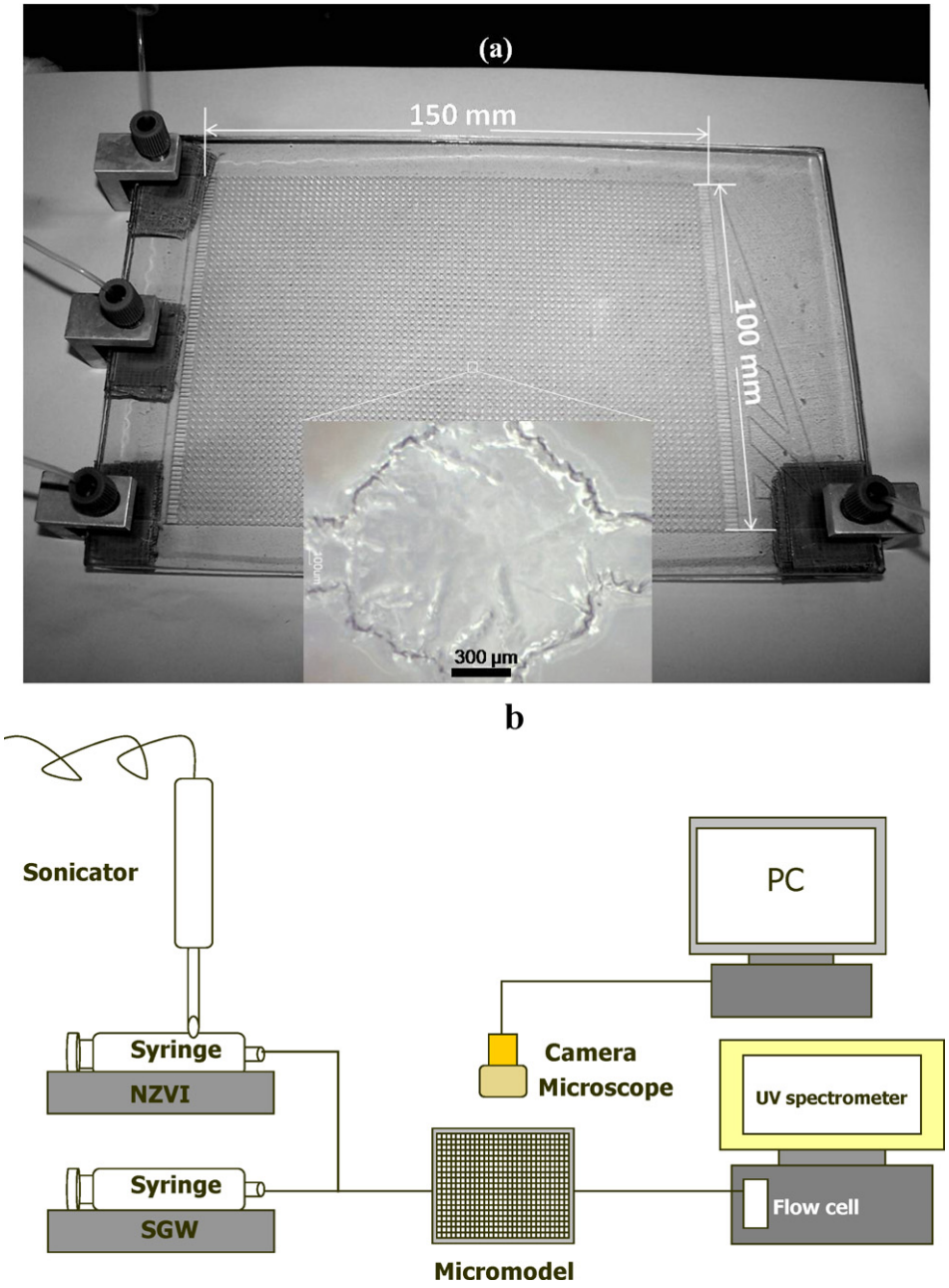

Fig. 1. (a) Micromodel pattern and (b) schematic of the experimental setup.

enhance the mobility of iron nanoparticles in groundwater [27,28]. However, the effects of the different characteristics of humic and fulvic acids on the kinetics and mechanisms of iron nanoparticle stabilization in porous media have not been reported. Similarly, there are no studies available on the visualization and quantification of the mobilization, aggregation, and deposition of iron nanoparticles that were stabilized using soil humic substances.

Quantification of nanoparticle deposition during transport through porous media has been difficult to obtain by column study although there have been a number of studies investigating the subsurface transport of nanosized materials [13,15,29]. Most previous studies have been limited to "black box" modeling based on the mass balance and breakthrough curves in packed sand columns [13,15,30–32]. No studies on the pore-scale visualization of iron nanoparticles transport in porous media have been reported. In addition, vertical flow of iron nanoparticles using a column filled with glass beads would not adequately represent the total pathways of nanoparticles movement in a groundwater aquifer [13]. In the subsurface, horizontal flow is also significant, however, there have only been a few studies about the behavior of groundwater flow in the horizontal direction [24,33]; the horizontal flow study of iron nanoparticles in porous media has never been reported. To this end, a micromodel investigation would enhance understanding of the pore-scale behavior of iron nanoparticles and thus would provide further insight into their macroscale behavior to explain the "black box" phenomenon in the column test.

The objectives of this study were: (1) to visualize the mobilization and deposition of iron nano and sub-micrometer particles (INSMP) under different particle and humic substance concentrations with a horizontally laid micromodel; (2) to explain the observed mobility enhancement of INSMP in the presence of NOM using the classical and extended DLVO theories.

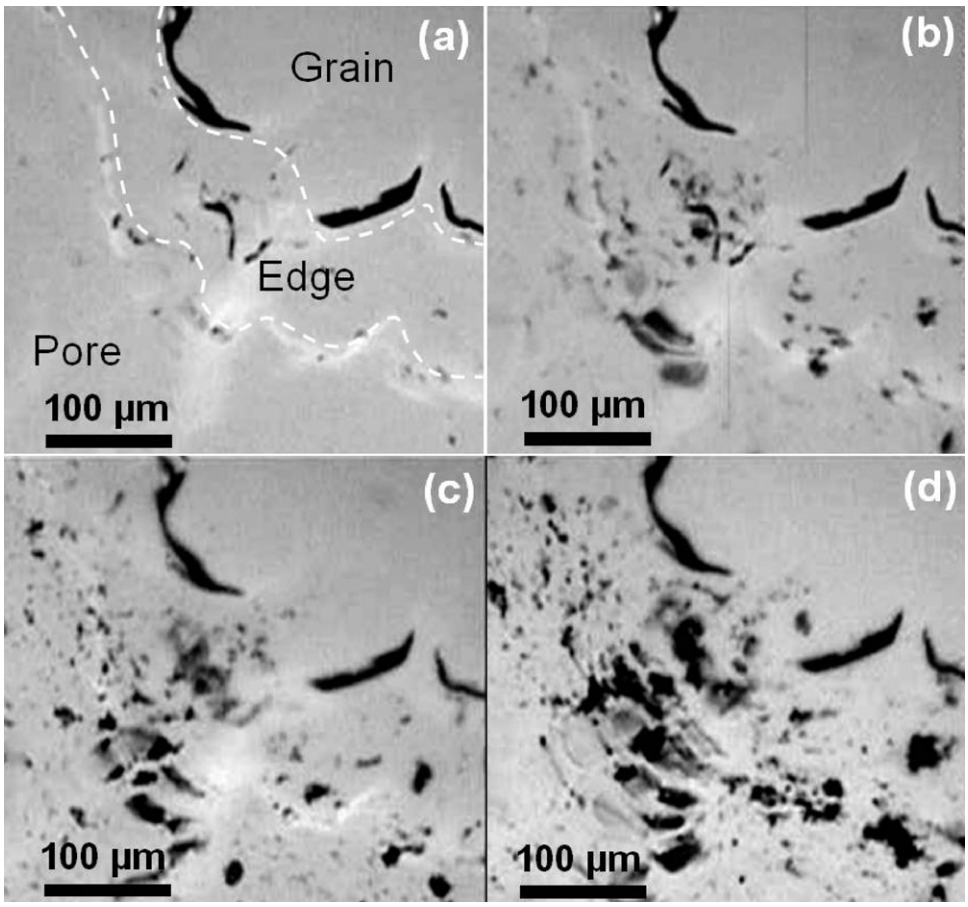

Fig. 2. Visualizations of INSMP deposition after one pore volume injection under different particle concentrations: (a) 0.05 g/L, (b) 0.1 g/L, (c) 0.15 g/L, and (d) 0.2 g/L, the flow rate is 4.59×10^{-4} m/s, and the background solution is DI water.

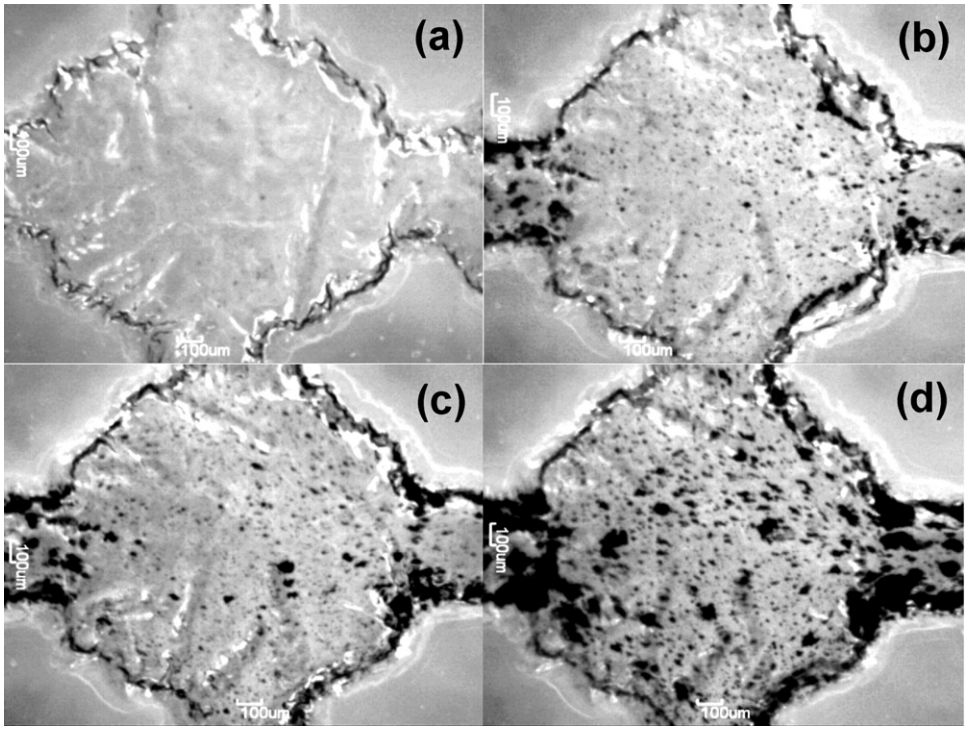

Fig. 3. Visualizations of INSMP depositions after six pore volumes injection under different particle concentrations in the micromodel: (a) 0.05 g/L, (b) 0.1 g/L, (c) 0.15 g/L, and (d) 0.2 g/L. The Darcy velocity is 4.59×10^{-4} m/s, and the background solution is DI water.

Table 1
Physical parameters held constant for micromodel.

Parameter		Value
2-D porous medium/(micromodel)	Length, L	150 mm
	Width, W	100 mm
	Collector diameter, d_c	1.3 mm
	Total porosity, ε	0.59
	Pore volume, V_p	2 mL
	Inner depth	200 μm
Temperature	25 ± 2 °C	
Flow rate for particles	10 mL/h, 2.295×10^{-4} m/s	
Flow rate for fluid approach	10 mL/h, 2.295×10^{-4} m/s	

2. Materials and methods

2.1. Chemicals

The chemicals used in this study ($NaBH_4$, $NaHCO_3$, KCl) were reagent grade obtained from Sigma–Aldrich (USA), and were used directly as received without pretreatment unless otherwise specified. In addition, $FeCl_3 \cdot 6H_2O$ and $CaCl_2 \cdot 2H_2O$ were obtained from Junsei (Japan), and $MgCl_2 \cdot 6H_2O$ was purchased from Oriental Chemical Industries (South Korea). The electrolyte stock solutions were prepared and then filtered through 0.45-μm filters (Advantec MFS, Inc.) before use. The iron nanoparticles were synthesized as described in previous studies [4,34]. The experiments and measurements were conducted in the synthetic groundwater (SGW) prepared similar to that of Dries et al. [35]: $NaHCO_3$, KCl, $CaCl_2$, and $MgCl_2$ (0.5 mM each), and pH were conducted at 7.0 ± 0.1; in addition, SGW was purged using nitrogen before experiments (DO value is less than 0.8 mg/L) [4]. Models for naturally occurring soil organic matter, Pahokee peat humic acid (PPHA, 1S103H standard I) and Pahokee peat fulvic acid (PPFA, 2S103F standard II), were purchased from the International Humic Substances Society (IHSS). All chemical stock solutions were prepared using doubly deionized (DI) water (18 MΩ Milli-Q) and stored at 4 °C prior to use. PPHA and PPFA background solutions were prepared by diluting these stock solutions into SGW with pH of 7.0 ± 0.1. The concentrations of the PPHA and PPFA in the prepared background solutions were confirmed using a total organic carbon analyzer (TOC-V_{CPH}, Shimadzu) based on the carbon content reported by the IHSS.

2.2. Micromodel configuration and experimental setup

This study used a well-defined porous medium for transport analysis of iron nanoparticles. A porous pattern-regularly-etched glass model allowed us to quantify and visualize the mobilization and deposition of iron nanoparticles during transport. Jeong et al. have described the detail configuration of this glass model [36]. The glass micromodel shown in Fig. 1(a) has a regular geometry with an average pore throat radius of 120 μm. The physical properties of the micromodel are summarized in Table 1.

A schematic of the experimental apparatus is shown in Fig. 1(b). The micromodel was horizontally mounted on the light stage of a microscope (iMegascope, EGVM-452M, with a 300× lens) that was equipped with a high resolution digital camera mounted directly on its eyepiece. Live images of the micromodel were displayed on a computer monitor. The captured images of the transport behavior of iron nanoparticles were analyzed using an image analyzer (IT Plus 5.0); additionally, prior to image analysis, the focus and resolution of the microscope were calibrated. The experimental setup allowed for the simultaneous injection of two different fluids: a T-shaped tube connector (Upchurch Scientific Co.) was connected by three PTFE tubes (2 mm OD × 1.5 mm ID). Two syringe pumps delivered iron nanoparticle aqueous solution and background solution, respectively. At the T-shape connector the separate fluids met and were then injected into the micromodel. A UV spectrometer was used for detecting the iron nanoparticle concentration in the effluent from the micromodel. In addition, high-resolution transmission electron microscope (TEM) analyses were performed to characterize the morphology of iron nanoparticles before injection into the micromodel. Surface charge (ζ-potential) and size distribution of iron nanoparticles were characterized using electrophoretic light

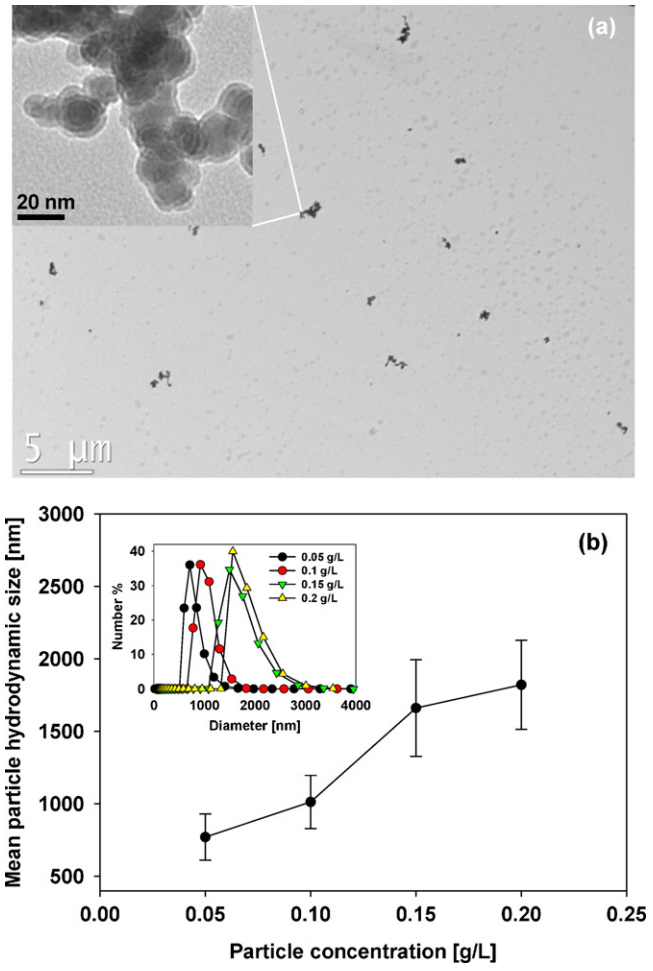

Fig. 4. (a) Transmission electron micrograph of INSMP suspension (0.05 g/L in DI water) showing aggregation of particles, inset is the high resolution TEM image of iron nanoparticles and (b) particle size distribution of INSMP under different particle concentrations based on ELS analysis.

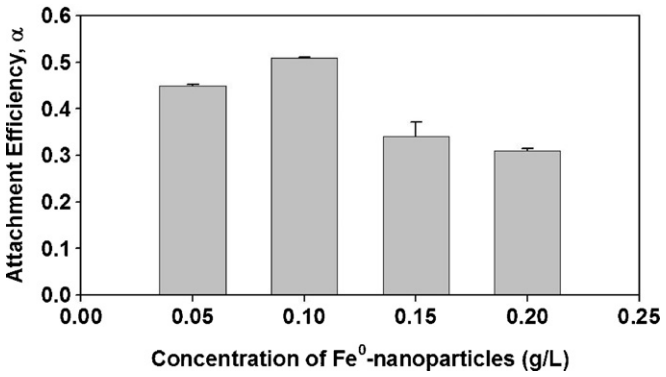

Fig. 5. Attachment efficiencies of INSMP under different particle concentrations in the micromodel.

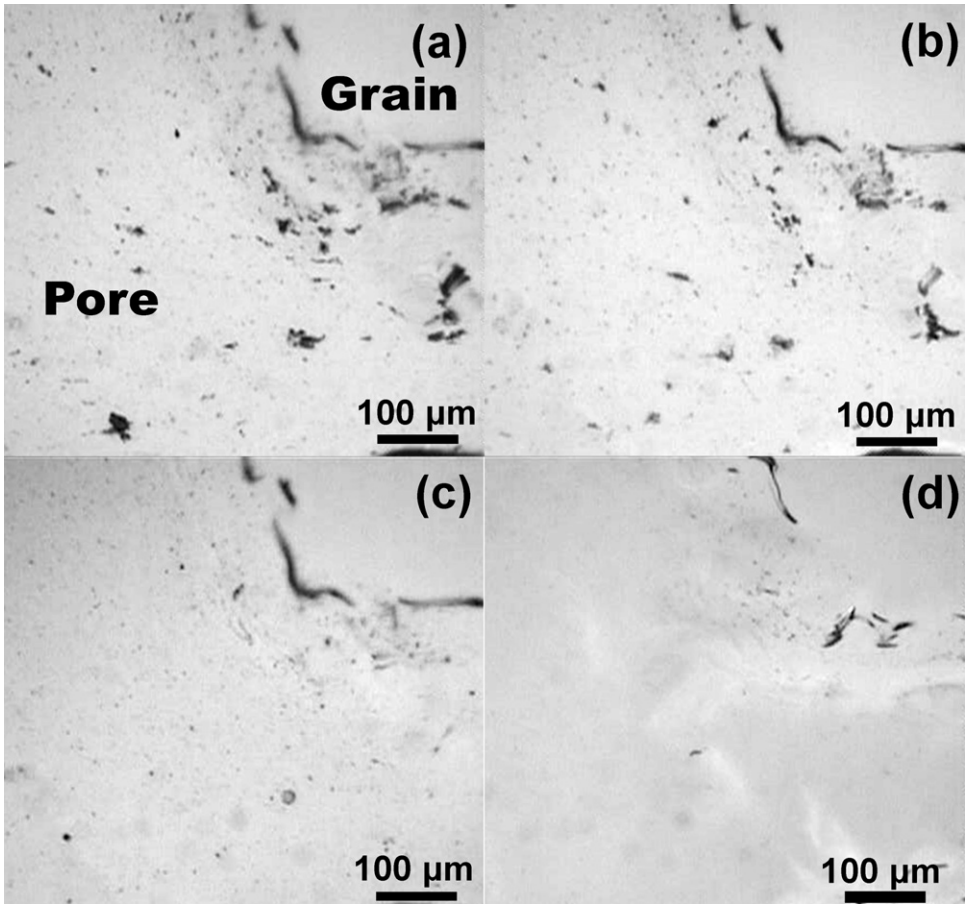

Fig. 6. Visualizations of INSMP depositions in SGW under different concentrations of PPHA after one pore volume injection: (a) 1 ppm, (b) 5 ppm, (c) 10 ppm, and (d) 15 ppm. The Darcy velocity is 4.59×10^{-4} m/s, $T = 25\,^{\circ}$C, pH = 7.0, and the concentration of INSMP is 0.05 g/L.

scattering (ELS-Z, version 2.2, Otsuka Electronics, Japan). All measurements were conducted at room temperature. The total iron and Fe^0 content in iron nanoparticle samples were subsequently determined using acid digestion method reported by Liu et al. [8].

2.3. Experimental procedure

The mobilization and deposition of iron nanoparticles in the micromodel were conducted using DI water and SGW solution. Before injecting iron nanoparticles, the micromodel was flushed with the background solution to provide a uniform collector surface charge. Iron nanoparticle suspensions in the background solutions were sonicated for 4 min in a sonication bath (B8510, Bransonic) and then continuously sonicated using a sonicator (VCX-400 Vibracell, Sonics and Materials, Inc.) during injection. Effluent samples from the micromodel were analyzed using a UV spectrophotometer (Mini 1240, Shimadzu) at 508 nm to determine the particle concentration [15].

3. Results and discussion

3.1. Visualization of the mobility of iron nano and sub-micrometer particles (INSMP) in porous media

Fate of iron nano and sub-micrometer particles (INSMP) in porous media was first visualized under continuous flow conditions. The background solution used here was DI water to know the effects of particle concentration on the mobility of INSMP. In our experiments, the bottom surface and edge of pores are rough [37], which can simulate real conditions in the subsurface porous media. Fig. 2(a–d) shows the visualizations of INSMP depositions near the pore edge of the micromodel after one pore volume injection; INSMP were densely deposited as the injection concentration increased. Also, note from Fig. 2(a) for the concentration of 0.05 g/L that a few aggregates were found on the bottom and edge of the pores. The visualized images of Fig. 2(c) and (d) showed that the depositions of INSMP for the concentrations of 0.15 and 0.2 g/L were greater than for lower concentrations, due both to interception and sedimentation as well as particle agglomeration from magnetic attractive forces [16].

From the pore-scale visualizations after six pore volume injections (Fig. 3), we easily observed that there were dense aggregations at the pores; these aggregates blocked the pores, which subsequently would decrease flow paths of the micromodel. Two regimes of iron-nanoparticle aggregation have been already demonstrated by Phenrat et al. under static conditions [16]. After big aggregates were generated in the aqueous solution under static conditions, they became new "collectors" – small particles attached onto these new collectors through diffusion, interception, and magnetic attraction. We observed similar phenomena even under continuous flow conditions as shown Figs. 2 and 3.

The visualization of the trajectory for INSMP sedimentation, interception, and detachment were described in Figs. S2–S4 (Supplementary material). Additionally, TEM image (Fig. 4a) showed aggregates with effective size less than 2 μm of INSMP under a concentration of 0.05 g/L prior to injection into the micromodel, while the intrinsic size of these particles was on the order of 20–40 nm (inset of Fig. 4a). The mean diameter and size distributions of INSMP

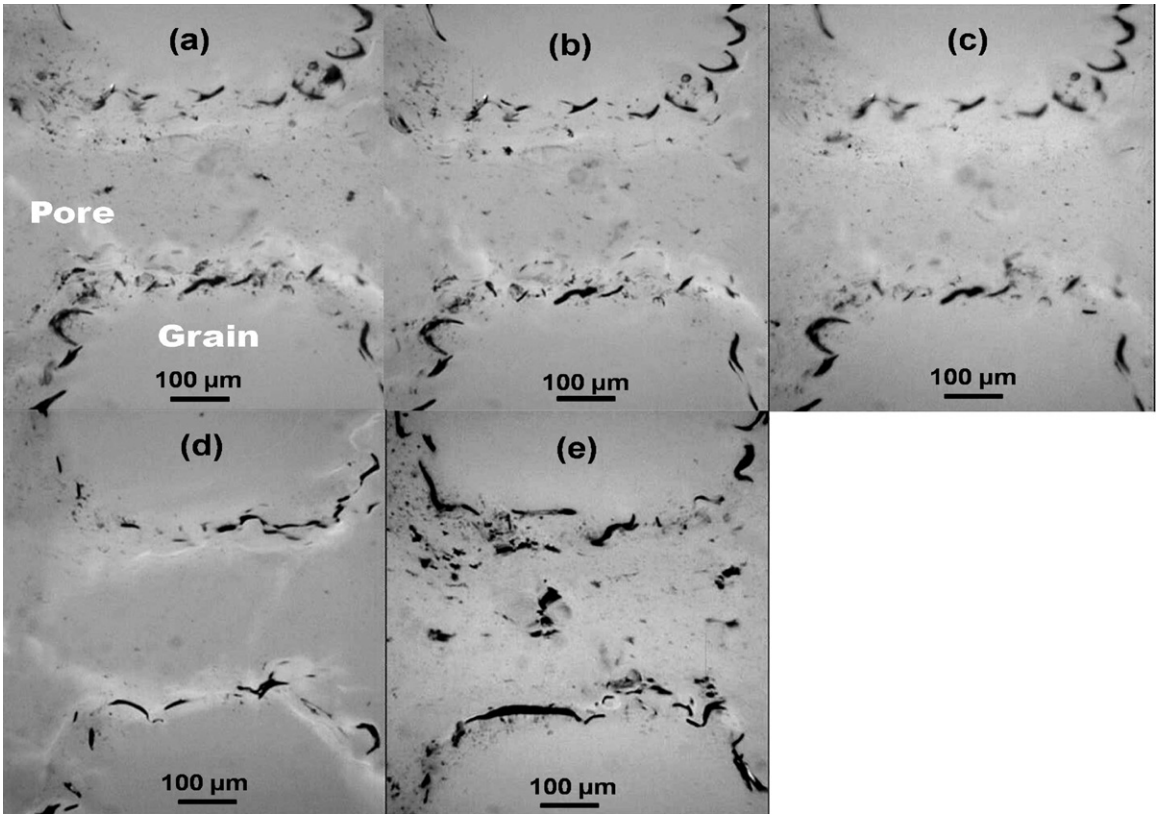

Fig. 7. Visualizations of INSMP depositions in SGW under different concentrations of PPFA after one pore volume injection: (a) 1 ppm, (b) 5 ppm, (c) 10 ppm, (d) 15 ppm, and (e) only SGW. The Darcy velocity is 4.59×10^{-4} m/s, $T = 25\,^{\circ}C$, pH = 7.0, and the concentration of INSMP is 0.05 g/L.

under different particle concentrations were shown in Fig. 4b. As the particle concentration increased from 0.05 g/L to 0.2 g/L, the hydrodynamic diameter was increased from 770.4 to 1820.9 nm. The observed results are consistent with visualizations taken from the micromodel, which confirmed that increasing particle concentration led to larger particle aggregation. Video (Supplementary material) image of these processes is available for further observation.

The attachment efficiencies, α, of different INSMP concentrations are shown in Fig. 5; the full theory expression of attachment efficiency is described in the Supplementary material. In Fig. 5, it can be seen that the attachment efficiency increased from 0.45 to 0.51 as the concentration increased from 0.05 to 0.1 g/L; however, the attachment efficiency decreased to 0.31, as the concentration increased to 0.2 g/L. Visualization results of INSMP fate were observed, contrary to attachment efficiency results using the deep bed filtration model, but consistent with the static condition results of Phenrat et al. [16]. The deep bed filtration model does not provide a complete representation of particle transport, such as partial coagulation caused by bridging and magnetic attractions among the INSMP [16,23]. As a result, the attachment efficiencies for concentrations of 0.15 and 0.2 g/L were likely to be underestimated comparing to visualization.

3.2. Effect of humic substances on the deposition of INSMP in porous media

The deposition of INSMP with a concentration of 0.05 g/L was investigated with background humic substances (PPHA and PPFA) in SGW at concentrations of 1, 5, 10, and 15 mg/L. Prior to these deposition experiments, the micromodel was rinsed with background solution for at least 40 pore volumes. Note that no significant UV absorbance value shifts were observed between the influent and effluent solutions, indicating that additional background humic substances would not adhere onto the micromodel inner surface after the saturated surface coating with background humic substances.

As shown in Table 2, the attachment efficiencies of 1 ppm PPHA (0.815 ± 0.006) and PPFA (0.782 ± 0.008) were a little higher than those without humic substances (0.778 ± 0.011). In the presence of $CaCl_2$ and $MgCl_2$, PPHA and PPFA were able to form complexes with Ca^{2+} and Mg^{2+}, which would result in macromolecules taking a more compact conformation. Also, some bridging would occur between the macromolecules on the INSMP and the inner surface of the micromodel [27]. However, as the concentrations of PPHA and PPFA in SGW were increased from 5 to 15 mg/L, a significant decrease in the attachment efficiency was observed (Table 2).

Mobility of INSMP in the presence of PPFA was higher than that for PPHA, showing that the attachment efficiency α_{PPFA} was less than α_{PPHA}. This observed result can be explained by structural reasons of humic substances: the specific UV absorbance ($SUVA_{254}$) and molecular weight distribution of PPFA are larger than those of PPHA (Fig. S5). The $SUVA_{254}$ is defined as the UV absorbance at 254 nm divided by the DOC concentration and is strongly correlated with the aromaticity of humic substances, more aromatic group content in humic substances directly enhancing the adsorption capacity [38]. Therefore, more PPFA molecules, comparing with PPHA molecules, can be adsorbed onto the surface of INSMP. Additionally, the observed result is similar to a previous reported study suggesting that the attraction interaction is higher between organic chemicals containing more aromatic groups and carbon nanotubes [39].

The electrophoretic mobility of INSMP in the SGW with PPHA and PPFA were then measured to determine the surface charge at pH 7. Our results confirmed that the surface charges of INSMP were more negative when in the presence of PPFA than when in the pres-

Table 2
Main parameters and results of total interaction energy calculations.

Particles/solution	Attachment efficiency (α)	Surface charge/zeta potential (mV)	Parameters in DLVO theory			
			Potential barrier height (kT)	Potential barrier distance from surface (nm)	Secondary minimum depth (kT)	Secondary minimum distance from surface (nm)
Fe^0-nanoparticles/SGW	0.773 ± 0.011	−12.125 ± 1.138	ND	ND	ND	ND
Fe^0-nanoparticles/PPHA (ppm)						
1	0.815 ± 0.006	−12.845 ± 0.629	-8.059×10^{-5}	14	−0.011	24
5	0.739 ± 0.004	−14.085 ± 1.294	0.047	11	-7.804×10^{-3}	28
10	0.689 ± 0.005	−15.290 ± 1.782	0.118	10	-6.184×10^{-3}	31
15	0.615 ± 0.008	−15.705 ± 0.516	0.146	9	-5.769×10^{-3}	32
Fe^0-nanoparticles/PPFA (ppm)						
1	0.782 ± 0.008	−13.855 ± 0.672	0.036	12	-8.214×10^{-3}	28
5	0.627 ± 0.003	−17.205 ± 0.389	0.281	8	-4.636×10^{-3}	34
10	0.560 ± 0.004	−18.305 ± 0.743	0.405	8	-4.060×10^{-3}	36
15	0.464 ± 0.006	−19.160 ± 0.269	0.517	7	-3.696×10^{-3}	37

ence of PPHA (Table 2). The surface charge of INSMP could cause more electrostatic repulsion among particles and between particles and inner surfaces of the micromodel in the presence of PPFA than it does with PPHA. Therefore, more aromaticity of PPFA significantly increases the steric and electrostatic repulsion of INSMP, as a result, the attachment efficiency was significantly decreased. These results suggest that naturally occurring NOM with concentrations of 0.7–15 mg/L could contribute to the mobility of INSMP, even under common groundwater conditions [28,40]. Visualizations for the depositions of INSMP under different concentrations of PPHA and PPFA are shown in Figs. 6 and 7. These visualizations further confirmed that deposition of INSMP in the micromodel decreased as the concentration of humic substances increased. Note from Fig. 7(e) that aggregates of iron nanoparticles were easily found under SGW condition without humic substances.

The mean diameter and particle size distributions of INSMP in the influent and effluent solutions were studied under different concentrations of humic substances (Fig. 8). The hydrodynamic diameter of INSMP suspended in PPHA and PPFA influent solutions were within the range of 755–936 nm and 540–908 nm, respectively; whereas those of effluent solutions were within the range of 420–709 nm and 360–654 nm, respectively. All processes, such as sedimentation, deposition, and interception of large/microscopic aggregations of INSMP, enhanced filtration of larger iron-nanoparticle aggregates inside the micromodel. Therefore, the size of INSMP in the effluent solution was smaller than that in the influent solution. The observed size results additionally showed that the INSMP size decreased in conjunction with increasing of $SUVA_{254}$, molecular weight distribution, and concentration of humic substances.

3.3. Application of classical and extended DLVO theories to the deposition of INSMP

In the interaction energy calculated by DLVO theories, the adsorption of humic substances increased electrostatic repulsion and steric interaction between particles, which result in higher repulsive energy barriers and shallower attractive secondary minima located at a greater separation distance (Table 2, Figs. S6 and S7). The detailed expressions of the classical and extended DLVO theories are described in the Supplementary material. These modifications of the total interaction energy profile would lead to less deposition and more detachment. Our experimental results also showed significant reduction in α (Table 2) and increase in the particle recovery fraction as the PPHA and PPFA concentration increased. The decrease in α for the presence of PPHA and PPFA should be attributed to both the increased energy barrier and the reduced depth of the secondary minimum. Here, the DLVO theory applies to single particle–particle interactions and not necessarily to particle–aggregate or aggregate–aggregate interactions, which are more complicated [16].

For magnetic nanoparticles such as iron nanoparticles, the magnetic attraction affected the interaction energy of a number of iron nanoparticles; additionally, in the extended DLVO theory there was no predicted energy barrier for aggregation (Figs. S6 and S7 dashed line). As a result, rapid aggregation of INSMP by magnetic attraction was observed for a number of particles. Note that steric or electrostatics interactions were not included in our calculations because there are no reliable expressions available for calculating them [21].

3.4. "Affinity transition" in the transport breakthrough curves of INSMP

Breakthrough curves of INSMP in SGW with PPHA and PPFA are presented in Fig. 9. Two striking departures from these break-

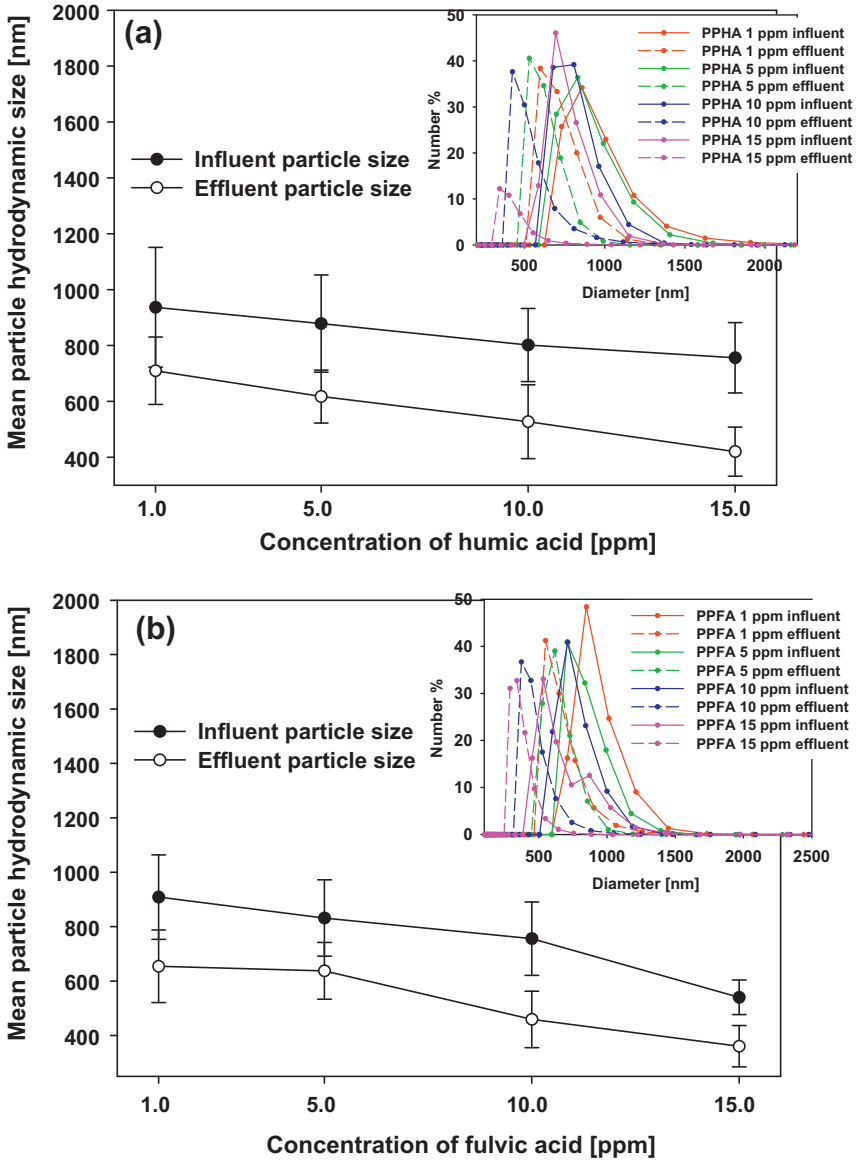

Fig. 8. Average hydrodynamic size of INSMP determined by electrophoretic light scattering (ELS-Z) for different concentrations of humic substances: (a) humic acid, (b) fulvic acid, and the inset is the particle size distribution (pH = 7.0 ± 0.1, at room temperature).

through curves were found; i.e., the breakthrough curve did not increase monotonously with the INSMP suspension flow through the micromodel. After a 1.5 pore volume injection, INSMP retention in the porous medium was observed to be steady, resulting in a constant effluent concentration. However, this apparent increase in the affinity of the porous medium for INSMP was temporary and the effluent concentration of INSMP then increased over third and fourth pore volume. After the fourth pore volume, the passage of INSMP through porous media reached another plateau. A similar "affinity transition" was observed in a column experiment using fullerene-based materials [30,41]. In our experiment, one possible explanation for the temporary plateau in the breakthrough curve observed during the second and third pore volume is based on the increased affinity of INSMP on the inner surface of the micromodel. However, INSMP retention in the porous medium was much longer compared with the "affinity transition" observed in the fullerene-based materials of the references. This observed phenomenon was likely due to the magnetic attraction between INSMP, which increased the attachment of INSMP onto the deposited INSMP aggregates.

An increased affinity condition would be produced through the modification of the collector inner surface as INSMP accumulate. The deposited INSMP would serve as favorable sites for subsequent INSMP deposition. This hypothesis was supported by consideration of the van der Waals forces between two particles and those between a particle and the inner surface of the micromodel [41]. The modification of the collector surface through INSMP deposition was predicted to lead to an increase in van der Waals forces between properly aligned INSMP and INSMP deposited on the collector surface.

After 2.5 and 3 pore volumes injection, the detachment of INSMP from the deposited INSMP became more obvious. This phenomenon leads to the second departure and second plateau in the breakthrough curves. In the second plateau, INSMP retention decreased with increasing concentrations of PPHA and PPFA (Fig. 9). As the PPHA and PPFA concentrations increased to 15 ppm, plateau (C/C_0) values of 0.31 and 0.42 respectively were reached after 4 pore volumes injection. As the PPHA and PPFA concentrations increased, an attractive secondary minimum decreased (Figs. S6 and S7), which is consistent with the observed decrease in INSMP retention

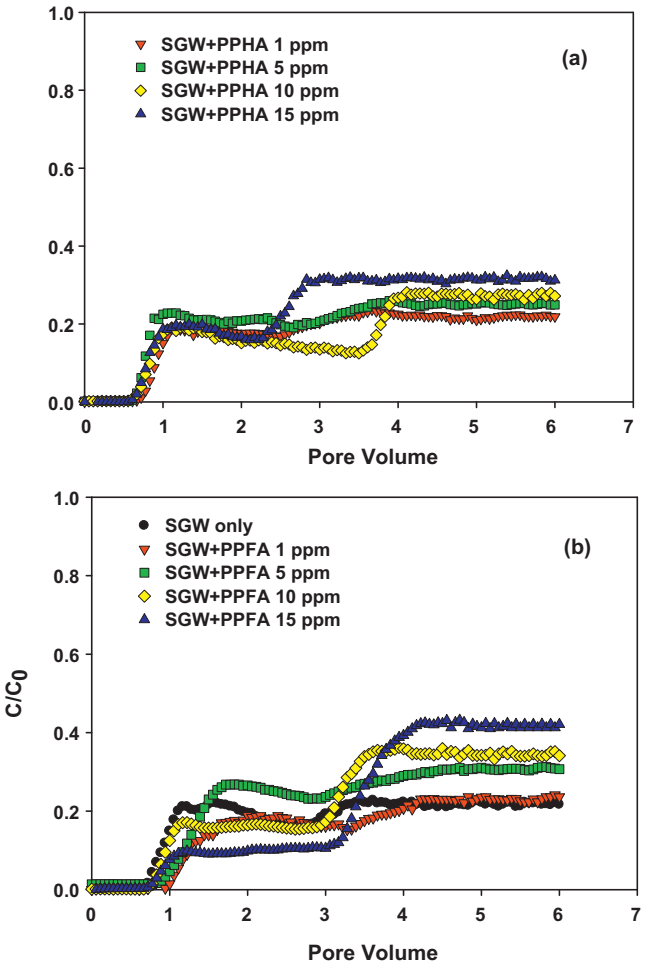

Fig. 9. Breakthrough curves of INSMP from the micromodel in the SGW with different concentrations of PPHA (a) and PPFA (b).

and increase in "affinity transition" in the micromodel. At the conditions where the PPHA and PPFA concentrations were decreased to 1 ppm, INSMP retention by the porous medium increased (showing reduced concentration ratios, $C/C_0 = 0.21$ and 0.23, respectively), thereby implying that repulsive interactions between the INSMP and collectors had been reduced.

4. Conclusions

Fate and transport of INSMP in porous media were successfully investigated using a glass micromodel. Understanding the aggregation behavior of INSMP in natural groundwater containing monovalent, divalent cations, and natural humic substances provides the key to predict their fate and transport in the subsurface. This study clearly showed that bare iron nanoparticles would form aggregates in the porous medium while flowing through pores, implying reduction in flow paths. Formation of INSMP aggregates in the pores was reduced in the presence of humic substances in the aqueous solution. The results of our study implied the "affinity transition" as well as the deposition and detachment of INSMP in groundwater were influenced by the concentration and properties of humic substances. For natural groundwater, the aromatic content and molecular weight distribution of humic substances would be important parameters to predict the extent of humic substances adsorption on INSMP and level of INSMP dispersion. In these simulations, the aggregation of INSMP in the presence of humic substances followed both the classical and extended DLVO type behaviors. In addition, high concentrations of humic substances increased the detachment of INSMP in the micromodel according to the increased energy barrier and reduced the depth of the secondary minimum.

Acknowledgments

This work was supported by the National Research Foundation grant funded by the Korea Government (2007-0056401), and Converging Technology Project funded by Korean Ministry of Environment.

Appendix A. Supplementary data

Supplementary data associated with this article can be found, in the online version, at doi:10.1016/j.jhazmat.2011.06.066.

References

[1] H. Choi, S.R. Al-Abed, S. Agarwal, D.D. Dionysiou, Synthesis of reactive nano-Fe/Pd bimetallic system-impregnated activated carbon for the simultaneous adsorption and dechlorination of PCBs , Chem. Mater. 20 (2008) 3649–3655.
[2] S.R. Kanel, B. Manning, L. Charlet, H. Choi, Removal of arsenic(III) from groundwater by nanoscale zero-valent iron , Environ. Sci. Technol. 39 (2005) 1291–1298.
[3] Y. Liu, H. Choi, D. Dionysiou, G.V. Lowry, Trichloroethene hydrodechlorination in water by highly disordered monometallic nanoiron , Chem. Mater. 17 (2005) 5315–5322.
[4] Q. Wang, S. Snyder, J. Kim, H. Choi, Aqueous ethanol modified nanoscale zerovalent iron in bromate reduction: synthesis, characterization, and reactivity , Environ. Sci. Technol. 43 (2009) 3292–3299.
[5] C. Su, R.W. Puls, Significance of iron (II,III) hydroxycarbonate green rust in arsenic remediation using zerovalent iron in laboratory column tests , Environ. Sci. Technol. 38 (2004) 5224–5231.
[6] S. Comba, A. Di Molfetta, R. Sethi, A comparison between field applications of nano-, micro-, and millimetric zero-valent iron for the remediation of contaminated aquifers , Water Air Soil Pollut. 215 (2011) 595–607.
[7] M. Gheju, Hexavalent chromium reduction with zero-valent iron (ZVI) in aquatic systems , Water Air Soil Pollut. (2011) (online first).
[8] Y. Liu, S.A. Majetich, R.D. Tilton, D.S. Sholl, G.V. Lowry, TCE dechlorination rates, pathways, and efficiency of nanoscale iron particles with different properties , Environ. Sci. Technol. 39 (2005) 1338–1345.
[9] S.M. Ponder, J.G. Darab, T.E. Mallouk, Remediation of Cr(VI) and Pb(II) aqueous solutions using supported, nanoscale zero-valent iron , Environ. Sci. Technol. 34 (2000) 2564–2569.
[10] W.-X. Zhang, Nanoscale iron particles for environmental remediation: an overview , J. Nanopart. Res. 5 (2003) 323–332.
[11] C. Noubactep, The fundamental mechanism of aqueous contaminant removal by metallic iron , Water SA (Online) 36 (2010) 663–670.
[12] C. Noubactep, S. Caré, On nanoscale metallic iron for groundwater remediation , J. Hazard. Mater. 182 (2010) 923–927.
[13] S.R. Kanel, D. Nepal, B. Manning, H. Choi, Transport of surface-modified iron nanoparticle in porous media and application to arsenic(III) remediation , J. Nanopart. Res. 9 (2007) 725–735.
[14] R. Lal, L. Lal, Encyclopedia of Soil Science , Taylor & Francis, Inc., 2005.
[15] N. Saleh, H.J. Kim, T. Phenrat, K. Matyjaszewski, R.D. Tilton, G.V. Lowry, Ionic strength and composition affect the mobility of surface-modified Fe-0 nanoparticles in water-saturated sand columns , Environ. Sci. Technol. 42 (2008) 3349–3355.
[16] T. Phenrat, N. Saleh, K. Sirk, R.D. Tilton, G.V. Lowry, Aggregation and sedimentation of aqueous nanoscale zerovalent iron dispersions , Environ. Sci. Technol. 41 (2007) 284–290.
[17] M. Elimelech, J. Gregory, X. Jia, R.A. Williams, Particle Deposition and Aggregation: Measurement, Modeling, and Simulation , Butterworth-Heinemann, Oxford, 1995.
[18] R. Rajamani, T. Chi, Trajectory analysis of deep-bed filtration with the sphere-in-cell porous media model , AICHE J. 22 (1976) 523–533.
[19] N. Tufenkji, M. Elimelech, Correlation equation for predicting single-collector efficiency in physicochemical filtration in saturated porous media , Environ. Sci. Technol. 38 (2004) 529–536.
[20] K.-M. Yao, M.T. Habibian, C.R. O'Melia, Water and waste water filtration. Concepts and applications , Environ. Sci. Technol. 5 (1971) 1105–1112.
[21] A. Franchi, C.R. O'Melia, Effects of natural organic matter and solution chemistry on the deposition and reentrainment of colloids in porous media , Environ. Sci. Technol. 37 (2003) 1122–1129.
[22] T. Phenrat, H.-J. Kim, F. Fagerlund, T. Illangasekare, R.D. Tilton, G.V. Lowry, Particle size distribution, concentration, and magnetic attraction affect transport of polymer-modified Fe0 nanoparticles in sand columns , Environ. Sci. Technol. 43 (2009) 5079–5085.

[23] Q. Wang, S.R. Kanel, H. Park, A. Ryu, H. Choi, Controllable synthesis, characterization and magnetic properties of nanoscale zerovalent iron with specific high Brunauer–Emmett–Teller surface area , J. Nanopart. Res. 11 (2009) 749–755.
[24] S.-W. Jeong, S.-D. Kim, Aggregation and transport of copper oxide nanoparticles in porous media , J. Environ. Monit. 11 (2009) 1595–1600.
[25] T. Phenrat, N. Saleh, K. Sirk, H.J. Kim, R.D. Tilton, G.V. Lowry, Stabilization of aqueous nanoscale zerovalent iron dispersions by anionic polyelectrolytes: adsorbed anionic polyelectrolyte layer properties and their effect on aggregation and sedimentation , J. Nanopart. Res. 10 (2008) 795–814.
[26] L. Weng, E.P.M.J. Fest, J. Fillius, E.J.M. Temminghoff, W.H. Van Riemsdijk, Transport of humic and fulvic acids in relation to metal mobility in a copper-contaminated acid sandy soil , Environ. Sci. Technol. 36 (2002) 1699–1704.
[27] K.L. Chen, M. Elimelech, Interaction of fullerene (C-60) nanoparticles with humic acid and alginate coated silica surfaces: measurements, mechanisms, and environmental implications , Environ. Sci. Technol. 42 (2008) 7607–7614.
[28] R.L. Johnson, G.O. Johnson, J.T. Nurmi, P.G. Tratnyek, Natural organic matter enhanced mobility of nano zerovalent iron , Environ. Sci. Technol. 43 (2009) 5455–5460.
[29] S.R. Kanel, R.R. Goswami, T.P. Clement, M.O. Barnett, D. Zhao, Two dimensional transport characteristics of surface stabilized zero-valent iron nanoparticles in porous media , Environ. Sci. Technol. 42 (2008) 896–900.
[30] J. Brant, H. Lecoanet, M.R. Wiesner, Aggregation and deposition characteristics of fullerene nanoparticles in aqueous systems , J. Nanopart. Res. 7 (2005) 545–553.
[31] H.F. Lecoanet, J.Y. Bottero, M.R. Wiesner, Laboratory assessment of the mobility of nanomaterials in porous media , Environ. Sci. Technol. 38 (2004) 5164–5169.
[32] J. Zhan, T. Zheng, G. Piringer, C. Day, G.L. McPherson, Y. Lu, K. Papadopoulos, V.T. John, Transport characteristics of nanoscale functional zerovalent iron/silica composites for in situ remediation of trichloroethylene , Environ. Sci. Technol. 42 (2008) 8871–8876.
[33] J. Zhuang, N. Goeppert, C. Tu, J. McCarthy, E. Perfect, L. McKay, Colloid transport with wetting fronts: Interactive effects of solution surface tension and ionic strength , Water Res. 44 (2010) 1270–1278.
[34] Q. Wang, S. Lee, H. Choi, Aging study on the structure of Fe0-nanoparticles: stabilization, characterization, and reactivity , J. Phys. Chem. C 114 (2010) 2027–2033.
[35] J. Dries, L. Bastiaens, D. Springael, S.N. Agathos, L. Diels, Competition for sorption and degradation of chlorinated ethenes in batch zero-valent iron systems , Environ. Sci. Technol. 38 (2004) 2879–2884.
[36] S.-W. Jeong, A.L. Wood, T.R. Lee, Enhanced contact of cosolvent and DNAPL in porous media by concurrent injection of cosolvent and air , Environ. Sci. Technol. 36 (2002) 5238–5244.
[37] S.-W. Jeong, M.Y. Corapcioglu, S.E. Roosevelt, Micromodel study of surfactant foam remediation of residual trichloroethylene , Environ. Sci. Technol. 34 (2000) 3456–3461.
[38] J.L. Weishaar, G.R. Aiken, B.A. Bergamaschi, M.S. Fram, R. Fujii, K. Mopper, Evaluation of specific ultraviolet absorbance as an indicator of the chemical composition and reactivity of dissolved organic carbon , Environ. Sci. Technol. 37 (2003) 4702–4708.
[39] H. Hyung, J.H. Kim, Natural organic matter (NOM) adsorption to multi-walled carbon nanotubes: effect of NOM characteristics and water quality parameters , Environ. Sci. Technol. 42 (2008) 4416–4421.
[40] J.A. Leenheer, M.A. Wilson, R.L. Malcolm, Presence and potential significance of aromatic-ketone groups in aquatic humic substances , Org. Geochem. 11 (1987) 273–280.
[41] H.F. Lecoanet, M.R. Wiesner, Velocity effects on fullerene and oxide nanoparticle deposition in porous media , Environ. Sci. Technol. 38 (2004) 4377–4382.